Confined states in ellipsoidal quantum dots

2000 J. Phys.: Condens. Matter 12 9019

(http://iopscience.iop.org/0953-8984/12/42/308)

J. Phys.: Condens. Matter **12** (2000) 9019–9036. Printed in the UK PII: S0953-8984(00)15964-8

Confined states in ellipsoidal quantum dots

G Cantele, D Ninno and G Iadonisi

Istituto Nazionale di Fisica della Materia and Dipartimento di Scienze Fisiche, Università di Napoli 'Federico II', Complesso Universitario Monte S Angelo, Via Cintia, I-80126 Napoli, Italy

Received 29 July 2000

Abstract. We study the motion of a particle confined in an ellipsoidal quantum dot, solving the corresponding Schrödinger equation both numerically, using the appropriate coordinate system, and variationally. The results from the two methods are compared, varying the ellipsoid semi-axes. We find that the confined-state energies split with respect to those of the spherical quantum dot and this can be explained as a consequence of both a volume-induced deformation effect and a geometry-induced one. The role of the dot geometry is shown to be relevant also for the formation of topological surface states.

1. Introduction

The interest in quantum dots and, more generally, semiconductor nanostructures has been growing in the last few years. The interesting feature of such structures is that as the system dimensions become smaller than the particle de Broglie wavelength, the physical properties are modified by quantum confinement. It is known, for example, that the optical gap increases on decreasing the mean dimensions, giving rise to a blue-shift of the optical spectra, and that a discrete set of states appears as an effect of reducing the system dimensionality. This has given rise to the possibility of a number of new, very interesting applications, such as producing artificial atoms and molecules [1], single-electron transistors [2] and quantum dot lasers [3]. The study of a quantum dot electronic structure can be done within several theoretical schemes, each one having advantages and drawbacks. There are semi-empirical calculations (tight binding, pseudopotential) [4–7] where the transferability of the bulk band-structure parameters to a nanostructure is assumed, first-principles calculations [8], which are computationally demanding, and the effective-mass approximation [9, 10], which has a high degree of flexibility but whose validity for very small nanostructures has been questioned. It has, indeed, been shown that the major causes of the confinement energy overestimation produced by the effective-mass approximation for very small quantum dots are band non-parabolicity contributions [10–13] and the hard-wall boundary conditions [14, 15]. It is therefore clear that when care is taken in choosing the lowest nanostructure dimension tractable within the effective-mass approximation [16], this method is a powerful tool for studying quantum confinement effects, particularly for those nanostructures where the shape plays an important role in determining the energy spectra [17].

Effective-mass calculations for nanostructure geometries characterized by particular symmetry properties [10] (for example spherical quantum dots or cylindrical quantum wires) have shown that the band-edge shift due to quantum confinement is the main cause of the

0953-8984/00/429019+18$30.00

experimentally observed optical properties. However, it must be stressed that the interpretation of these properties as a function of only the system 'mean dimensions' (that is, of its volume) is correct, to a good approximation, for systems that are sufficiently isotropic. When the system geometry begins to show a certain degree of anisotropy, it is not enough to know its 'mean dimensions' in order to describe its physical properties. In other words, if the system loses some symmetry because of a certain shape deformation, the effect of confinement can be understood only if related to the geometry changes. The dependence of the energy level structure and optical spectra on the system anisotropy has been investigated, for example, for InAs self-assembled quantum dots with lateral dimensions very different from their height [18, 19]. The results show a splitting in the conduction band excited states with respect to the case of a rotationally invariant system. A similar splitting effect has been investigated also for vertical circular, elliptic and triangular quantum dots fabricated in semiconductor hetero-interfaces [20]. Moreover, Efros and Rodina [21] have considered CdSe ellipsoidal quantum dots taking into account the fourfold degeneracy of the top valence band. The calculations include the ellipticity as a perturbation on the spherical eigenstates.

In this paper we shall show that it is possible to avoid using perturbation theory and determine the exact single-particle spectra. We shall limit ourselves to conduction band states, although an extension of our calculations to valence states with the inclusion of fourfold degeneracy could be considered. Given the mathematical complexity of the problem, we shall only report on single-particle properties. Electron–electron interaction effects and their relation to Coulomb blockade, excitons and the related optical properties will be discussed in future works.

Our main result is that if ellipsoidal quantum dots are considered instead of the spherical ones, the energy spectrum modifies as a function of the system anisotropy and that this result cannot be obtained if only the 'mean dimensions' are considered. Moreover, with the aim of giving a complete description of all types of geometry-induced confinement in an ellipsoidal quantum dot, we also present the results of calculations for a new type of surface state—that is, states whose localization is related to the surface curvature [22–24]. We show that the surface wave function does localize at different points according to the actual dot eccentricity. A comparison with the corresponding volume-confined states is made.

In section 2 we show how to exactly solve the free-particle Schrödinger equation within an ellipsoidal quantum dot using hard-wall boundary conditions and a coordinate system in which it is separable. In section 3 it is shown that it is possible to give also a functional variational formulation for the problem in order to avoid the mathematical difficulties involved in the exact solution. This approach is very general when small shape deformations with respect to a symmetrical geometry are considered [25]. In section 4 we illustrate the nature of the topological surface states, deriving the relevant equations. Finally, in section 5 we give the numerical results obtained for both volume and topological surface states, and in section 6 we draw some conclusions.

2. Volume-confined states

In this section we want to show how to calculate eigenfunctions and eigenvalues of a particle confined in a closed region of space with ellipsoidal geometry. Let us consider an ellipsoidal quantum dot with rotational symmetry around the z-direction. We will indicate as a and c its semi-axes along the x–y plane and the z-direction respectively (x, y and z are the coordinates in a Cartesian orthogonal system with its origin at the ellipsoid symmetry centre). The region

considered is limited by the surface S with parametric equations

$$\begin{aligned} x &= a\cos\Phi\sin\Theta \\ y &= a\sin\Phi\sin\Theta \\ z &= c\cos\Theta \end{aligned} \tag{1}$$

with $0 \leqslant \Phi < 2\pi$ and $0 \leqslant \Theta \leqslant \pi$. Our problem is that of solving the free-particle Schrödinger equation

$$-\frac{\hbar^2}{2m^*}\vec{\nabla}^2\Psi(x, y, z) = E^v\Psi(x, y, z) \tag{2}$$

(where m^* is the particle mass and E^v its energy) with the boundary condition

$$\Psi(x, y, z)\big|_{(x,y,z)\in S} = 0. \tag{3}$$

It is therefore necessary to find a new coordinate system (ξ, η, Φ) such that equation (2) is separable and such that the equation of our surface S in the new coordinate system reads $\xi =$ constant. Let us consider the following transformation (prolate spheroidal coordinates [26]):

$$\begin{aligned} x &= f\sqrt{(\xi^2-1)(1-\eta^2)}\cos\Phi \\ y &= f\sqrt{(\xi^2-1)(1-\eta^2)}\sin\Phi \\ z &= f\xi\eta \end{aligned} \tag{4}$$

where $1 \leqslant \xi < +\infty$, $-1 \leqslant \eta \leqslant +1$, $0 \leqslant \Phi < 2\pi$ and f is a parameter. Setting $\eta = \cos\Theta$ with $0 \leqslant \Theta \leqslant \pi$, equation (4) shows that the surfaces $\xi =$ constant represent a family of ellipsoids with semi-axes $f\sqrt{\xi^2-1}$ and $f\xi$ (along the x–y plane and the z-direction respectively), all characterized by the same focal distance $2f$. Therefore, the parameter f is determined by the condition that our ellipsoid belongs to this surfaces family—that is, there must exist a value $\overline{\xi}$ of ξ such that

$$\begin{cases} f\sqrt{\overline{\xi}^2-1} = a \\ f\overline{\xi} = c \end{cases} \Rightarrow \begin{cases} f = c\sqrt{1-\dfrac{1}{\chi^2}} = ce \\ \overline{\xi} = \dfrac{1}{\sqrt{1-\dfrac{1}{\chi^2}}} = \dfrac{1}{e} \end{cases} \tag{5}$$

where $\chi = c/a$ and $e = f/c$ is the ellipsoid eccentricity. It is evident that equation (5) is valid only if $\chi > 1$, which follows from the fact that the transformation (4) parametrizes the space with ellipsoidal surfaces which have the semi-axis along the z-direction greater than the semi-axis along the x–y plane. We will discuss the case $\chi < 1$ later.

It is now possible to write equation (2) in the new coordinate system [27]:

$$-\frac{1}{\sqrt{\det\mathbf{G}}}\sum_{i,j=1}^{3}\frac{\partial}{\partial q_i}\left[\overline{G}_{i,j}\sqrt{\det\mathbf{G}}\,\frac{\partial}{\partial q_j}\Psi(q_1, q_2, q_3)\right] = \varepsilon^v\Psi(q_1, q_2, q_3) \tag{6}$$

where $\mathbf{G} \equiv (G_{i,j}) = (\partial\vec{r}/\partial q_i \cdot \partial\vec{r}/\partial q_j)$ is the metric tensor, $\overline{G}_{i,j}$ the ratio between the algebraic complement of $G_{i,j}$ and $\det\mathbf{G}$, $(q_1, q_2, q_3) \equiv (\xi, \eta, \Phi)$ and $\varepsilon^v = 2m^*E^v/\hbar^2$. Using

equation (4) it is not difficult to show that

$$\begin{aligned} G_{1,1} &= f^2\frac{\xi^2-\eta^2}{\xi^2-1} \\ G_{2,2} &= f^2\frac{\xi^2-\eta^2}{1-\eta^2} \\ G_{3,3} &= f^2(\xi^2-1)(1-\eta^2) \end{aligned} \tag{7}$$

while $G_{i,j}=0$ for $i\neq j$ (that is, the new coordinate system is orthogonal). It is easy to show that equation (6) can be solved with the separation-of-variables technique. In other words, we can write its solution as $\Psi(\xi,\eta,\Phi)=J(\xi)S(\eta)\exp(\mathrm{i}m\Phi)$, where we have taken into account the fact that, because of the rotational symmetry around the z-direction, it is possible to find a complete set of solutions of equation (2) which are simultaneously eigenfunctions of the z-component of the angular momentum with eigenvalues $m\hbar$ ($m=0,\pm1,\pm2,\ldots$). In this way equation (6) separates into two equations (for J and S respectively):

$$\frac{\mathrm{d}}{\mathrm{d}\xi}\left[(\xi^2-1)\frac{\mathrm{d}J}{\mathrm{d}\xi}\right]-\left(A-h^2\xi^2+\frac{m^2}{\xi^2-1}\right)J=0 \tag{8a}$$

$$\frac{\mathrm{d}}{\mathrm{d}\eta}\left[(1-\eta^2)\frac{\mathrm{d}S}{\mathrm{d}\eta}\right]+\left(A-h^2\eta^2-\frac{m^2}{1-\eta^2}\right)S=0 \tag{8b}$$

which are formally equal but must be solved for different ranges of the respective variables (that is, $1\leqslant\xi<+\infty$ and $-1\leqslant\eta\leqslant1$). A represents the separation constant and $h=f\sqrt{\varepsilon^v}$. We can notice that equations (8*a*) and (8*b*) are coupled by both the separation constant and h. Therefore, the separation of the Schrödinger equation in spheroidal coordinates is more difficult than in spherical or cylindrical coordinates. In fact, in these latter cases only the first equation contains h, so one can solve the second equation determining the A-values in such a way that its solutions are finite in the corresponding interval, substitute these values in the first equation and then solve it to get the allowed energies levels. In our case we follow the same procedure, but the second equation must be solved with fixed h so that the discrete A-values, obtained by imposing the finiteness of the solution at the points -1 and $+1$, are functions of h. It must be pointed out that if $h\to0$ (that is, $f\to0$) the prolate spheroidal coordinates tend to spherical coordinates (because the surfaces $\xi=$ constant become ellipsoids with very small focal distances). A direct consequence is that if we consider equation (8*b*) as $h\to0$, we must obtain $S(\eta)\to P_l^{|m|}(\eta)$ (where $P_l^{|m|}(\eta)$ are the associated Legendre functions) and $A\equiv A(h)\to l(l+1)$ with $l=|m|,|m|+1,|m|+2,\ldots$. Therefore it is possible to label the solutions of equation (8*b*) and the corresponding values of the separation constant as $S(\eta)\equiv S_{l,m}(h,\eta)$ and $A\equiv A_{l,m}(h)$ with $|m|=0,1,2,\ldots$ and $l=|m|,|m|+1,|m|+2,\ldots$. Correspondingly we can set for equation (8*a*) $J(\xi)\equiv je_{l,m}(h,\xi)$. It can be shown [26] that the solutions of equation (8*a*) and (8*b*) can be written respectively as

$$je_{l,m}(h,\xi)=\left(\frac{\xi^2-1}{\xi^2}\right)^{|m|/2}{\sum_{s=0,1}^{+\infty}}' a_s^{l,m}(h)\,j_{s+|m|}(h\xi) \tag{9}$$

and

$$S_{l,m}(h,\eta)={\sum_{s=0,1}^{+\infty}}' d_s^{l,m}(h)\,P_{s+|m|}^{|m|}(\eta) \tag{10}$$

where j_k is the spherical Bessel function of order k. The primed sum indicates that the sum must be extended over even values or odd values of s in which cases it begins from 0 and 1 respectively. This reflects the system invariance with respect to parity transformations. It

is possible to derive the coefficient recurrence formulae and the expansions of the separation constant $A_{l,m}$ as $h \to 0$ and $h \to +\infty$, inserting the series (9) and (10) in the respective equations. Some more details are given in the appendix.

If $c < a$ (that is, $\chi < 1$) it is possible to follow the same procedure as indicated above but using oblate spheroidal coordinates [28]:

$$\begin{aligned} x &= f\sqrt{(\xi^2+1)(1-\eta^2)}\cos\Phi \\ y &= f\sqrt{(\xi^2+1)(1-\eta^2)}\sin\Phi \\ z &= f\xi\eta \end{aligned} \tag{11}$$

with $0 \leqslant \xi < +\infty$, $-1 \leqslant \eta \leqslant +1$ and $0 \leqslant \Phi < 2\pi$. The surfaces $\xi =$ constant represent a family of ellipsoids with semi-axes $f\sqrt{\xi^2+1}$ and $f\xi$ (the semi-axis along the x–y plane is in this case greater than the one along the z-direction). Equation (5) becomes

$$\begin{cases} f\sqrt{\bar{\xi}^2+1} = a \\ f\bar{\xi} = c \end{cases} \Rightarrow \begin{cases} f = c\sqrt{\dfrac{1}{\chi^2}-1} = ae \\ \bar{\xi} = \dfrac{1}{\sqrt{\dfrac{1}{\chi^2}-1}} = \dfrac{\chi}{e} \end{cases} \tag{12}$$

with $\chi < 1$. The diagonal components of the metric tensor are

$$\begin{aligned} G_{1,1} &= f^2\frac{\xi^2+\eta^2}{\xi^2+1} \\ G_{2,2} &= f^2\frac{\xi^2+\eta^2}{1-\eta^2} \\ G_{3,3} &= f^2(\xi^2+1)(1-\eta^2) \end{aligned} \tag{13}$$

while the non-diagonal ones are null. Equation (6) separates into two equations:

$$\frac{\mathrm{d}}{\mathrm{d}\xi}\left[(\xi^2+1)\frac{\mathrm{d}J}{\mathrm{d}\xi}\right] - \left(A - h^2\xi^2 - \frac{m^2}{\xi^2+1}\right)J = 0 \tag{14a}$$

$$\frac{\mathrm{d}}{\mathrm{d}\eta}\left[(1-\eta^2)\frac{\mathrm{d}S}{\mathrm{d}\eta}\right] + \left(A + h^2\eta^2 - \frac{m^2}{1-\eta^2}\right)S = 0 \tag{14b}$$

which must be solved for different ranges of the respective variables (that is, $0 \leqslant \xi < +\infty$ and $-1 \leqslant \eta \leqslant 1$). The solutions can be written using expansions (9) (provided that in this equation we make the substitution $(\xi^2-1)/\xi^2 \to (\xi^2+1)/\xi^2$) and (10) again but, as we show in the appendix, the expansions of the separation constant $A_{l,m}$ as $h \to 0$ and $h \to +\infty$ are different from the case of prolate spheroidal coordinates.

The solution of equation (8*a*) or equation (14*a*) (depending on whether $\chi > 1$ or $\chi < 1$ respectively) with the additional condition $je_{l,m}(h, \bar{\xi}) = 0$ (hard-wall boundary condition) gives the discrete spectrum $\varepsilon^v_{n,l,m} = 2m^* E^v_{n,l,m}/\hbar^2$ of the particle confined in the ellipsoidal quantum dot. The label $n = 1, 2, 3\ldots$ takes into account the fact that for fixed l and m the boundary condition can be compatible with a discrete set of values of h. We expect our solutions to go into the spherical ones for $\chi \to 1$. Let us remember that for the sphere a complete set of eigenfunctions is given by $\Psi^0_{n,l,m}(r, \vartheta, \varphi) = j_l\left[z_{n,l}(r/R)\right]Y^m_l(\vartheta, \varphi)$ where r, ϑ, φ are the spherical coordinates of the generic point, R is the sphere radius, $z_{n,l}$ the nth zero of the Bessel function of order l and $Y^m_l(\vartheta, \varphi)$ the spherical harmonics ($Y^m_l(\vartheta, \varphi) \propto P^{|m|}_l(\cos\vartheta)\exp(\mathrm{i}m\varphi)$). This state has energy $\varepsilon^0_{n,l} = z^2_{n,l}/R^2$, which is degenerate with respect to m. We can label the

energy levels ns, np, nd, ..., where s, p, d, ... correspond to $l = 0, 1, 2, \ldots$ respectively. From the mathematical point of view, n and $l - m$ are related to the number of nodes respectively of the radial part and the angular part of the wave function inside the sphere. Moreover, $l(l+1)\hbar^2$ takes the physical meaning of the total angular momentum of the particle in the given quantum state, reflecting the full rotational symmetry of the problem. This, of course, is no longer true for the ellipsoid quantum states because this type of symmetry is lost. It is therefore important to stress that if $\chi \neq 1$, the label l which appears in equations (9) and (10) does not have the meaning of the total angular momentum of the particle. It has been used here because there obviously exists a one-to-one correspondence between the quantum states in the sphere and the ones in the ellipsoid, so these latter can be labelled with the same quantum number as the state to which they reduce when $f \to 0$.

3. The variational approach for the volume-confined states

As we have seen in the previous section, the exact solution of the problem of a particle confined in an ellipsoidal volume is very difficult, mainly because the two equations resulting from the variable separation are coupled by both the eigenvalue and the separation constant. It is therefore interesting to try to get approximate evaluations of the particle wave functions and allowed energies using, for example, a variational approach.

Because the ground-state trial function $\widetilde{\Psi}_0(r, \vartheta, \varphi)$ must reduce to $\Psi^0_{1,0,0}(r, \vartheta, \varphi)$ in the limit $\chi \to 1$, we can set

$$\widetilde{\Psi}_0(r, \vartheta, \varphi) = j_0\left[\frac{\pi}{R(\vartheta)} r\right] f(\vartheta) \tag{15}$$

where

$$R(\vartheta) = c/\sqrt{\chi^2 + (1 - \chi^2)\cos^2\vartheta}$$

represents the distance of the generic point of the ellipsoid surface from its centre. It must be pointed out that we are using in this case spherical coordinates r, ϑ, φ. In equation (15) we have considered that for the ground state we have $l = m = 0$, that $z_{1,0} = \pi$ (so that the wave function vanishes on the boundary $r = R(\vartheta)$) and that, because our problem is now invariant for rotations only around the z-direction, the ground state does not depend on φ. The function $f(\vartheta)$ in equation (15) takes into account the deformation effects which the ellipsoidal geometry induces with respect to the completely symmetric spherical case. The function $f(\vartheta)$ has to be determined in such a way that the energy functional

$$\widetilde{E}^v[f] = \frac{\langle\widetilde{\Psi}_0|-(\hbar^2/2m^*)\,\vec{\nabla}^2|\widetilde{\Psi}_0\rangle}{\langle\widetilde{\Psi}_0|\widetilde{\Psi}_0\rangle} \tag{16}$$

is stationary with respect to an arbitrary variation of f. This, according to the variational principle, gives an upper bound to the ground-state energy. Taking the variation of equation (16) with respect to f, we obtain that

$$\langle\widetilde{\Psi}_0|\widetilde{\Psi}_0\rangle\,\delta\widetilde{E}^v[f] + (\langle\widetilde{\Psi}_0|\delta\widetilde{\Psi}_0\rangle + \text{c.c.})\widetilde{E}^v[f] = (\langle\widetilde{\Psi}_0|-(\hbar^2/2m^*)\,\vec{\nabla}^2|\delta\widetilde{\Psi}_0\rangle + \text{c.c.}) \tag{17}$$

where c.c. indicates the complex conjugate of the corresponding term in parentheses and $\delta\widetilde{\Psi}_0 = j_0[\pi r/R(\vartheta)]\,\delta f(\vartheta)$. The stationarity of the functional (16) with respect to this variation of $f(\vartheta)$ is given by the condition $\delta\widetilde{E}^v[f] = 0$. Moreover, because the variation $\delta f(\vartheta)$ is a function just of ϑ, we can compute in equation (17) the integrals with respect to φ

and r. The final equation, which follows from simple algebraic manipulations and considering that $\delta f(\vartheta)$ is arbitrary, is

$$-\frac{\mathrm{d}}{\mathrm{d}\vartheta}\left(\sin\vartheta\,\frac{\mathrm{d}f}{\mathrm{d}\vartheta}\right)+\frac{\pi\sin\vartheta}{2\,\mathrm{Si}(2\pi)}\left[1+\frac{(\mathrm{d}R/\mathrm{d}\vartheta)^2}{R^2(\vartheta)}\right]f(\vartheta)=\widetilde{\varepsilon}^{v}\frac{(\sin\vartheta)R^2(\vartheta)}{2\pi\,\mathrm{Si}(2\pi)}f(\vartheta) \tag{18}$$

where $\mathrm{Si}(u)=\int_0^u[(\sin\rho)/\rho]\;\mathrm{d}\rho$ and $\widetilde{\varepsilon}^{v}=2m^*\widetilde{E}^{v}/\hbar^2$. Equation (18) must be solved with the condition

$$\langle\widetilde{\Psi}_0|\widetilde{\Psi}_0\rangle=\int_0^{\pi}(\sin\vartheta)\frac{R^3(\vartheta)}{\pi}f^2(\vartheta)\,\mathrm{d}\vartheta=1. \tag{19}$$

For $\chi\to 1$ (that is, $R(\vartheta)\to R$ constant) equation (18) admits the solution $f(\vartheta)=$ constant with $\widetilde{\varepsilon}^{v}=\pi^2/R^2$—that is, the ground-state energy for the sphere, as expected. Finally, equation (18) contains a term in the first derivative of $f(\vartheta)$ which can be eliminated by setting $f(\vartheta)=g(\vartheta)/\sqrt{\sin\vartheta}$. This leads to

$$-\frac{\mathrm{d}^2g}{\mathrm{d}\vartheta^2}+\left\{\frac{\pi}{2\,\mathrm{Si}(2\pi)}\left[1+\frac{(\mathrm{d}R/\mathrm{d}\vartheta)^2}{R^2(\vartheta)}\right]-\frac{1}{4\sin^2\vartheta}-\frac{1}{4}\right\}g(\vartheta)=\widetilde{\varepsilon}^{v}\frac{R^2(\vartheta)}{2\pi\,\mathrm{Si}(2\pi)}g(\vartheta) \tag{20}$$

which shows that the confinement of the particle in the ellipsoid can be viewed as the motion in an effective ϑ-dependent potential. The particle in this picture behaves as if it had a position-dependent effective mass $\widetilde{m}(\vartheta)=m^*R^2(\vartheta)/2\pi\,\mathrm{Si}(2\pi)c^2$.

4. Topological surface states

In a previous work [22] we have shown that if a particle is confined in the neighbourhood of a nanostructure surface, then states localized along the surface can arise. This localization is induced by surface curvature; that is, on a flat surface a particle can move freely whereas on an undulating surface the particle may be trapped. The potential acting on the direction normal to the surface whose role is that of keeping the particle in the surface neighbourhood may have different physical origins. It is beyond the scope of this paper to enter into details on how such a potential may be built, but a physical hint can easily be given. When a nanostructure is exposed to an oxidizing or reducing gas, a distribution of surface dielectric dipoles can be induced whose overall effect may be that of giving a potential pushing the particle toward the surface [29]. Another instance is surely that of an accumulation layer, in particular that corresponding to the steepest band slope with an extent of a few nanometres. Such layers may be found in both two-dimensional systems [30] and nanostructures [31].

The surface states that we are going to study represent a new kind of state because they are not associated with the breaking of the lattice periodicity or with electronic surface defects. The confinement of the particle near the surface gives rise to a topological potential which confines it to the points of largest curvature. This result has been obtained for non-limited structures such as a deformed quantum wire [22]. In that case, a surface mini-band structure appears, with confined (that is, non-extended) surface states below the mini-band edges. Moreover, it has also been shown that the surface mini-band edges are located below the volume-confined lowest mini-band edge. The most interesting feature of these states is that the surface trapping of electrons and/or holes could both open new channels for optical emission and/or absorption and modify the electrical conductivity of the material.

In this section we want to show that topological surface states can arise also on an ellipsoidal closed surface, as one would expect because of their very general nature. In the following we shall just outline the derivation of the relevant equations, the mathematical details being presented in references [22], [23] and [24].

Let us suppose that there exists a potential which confines the particle in the surface neighbourhood. If the surface parametric equations are $\vec{r} = \vec{r}(q_1, q_2)$, it is possible to identify a point in the neighbourhood of the surface with the vector $\vec{R}(q_1, q_2, q_3) = \vec{r}(q_1, q_2) + q_3\vec{N}(q_1, q_2)$, where $\vec{N}(q_1, q_2)$ is the normal to the surface and q_3 represents the algebraic distance of the point from the surface. In this way we can define a local curvilinear coordinate system (q_1, q_2, q_3) and write the Schrödinger equation in this new system. It has in particular been shown that, if the potential is sufficiently attractive, it is possible to separate the motion along the surface from the motion along its normal, defining a surface probability density $\sigma(q_1, q_2)$ ($|\sigma(q_1, q_2)|^2\,\mathrm{d}S$ represents the probability of finding the particle in the surface element $\mathrm{d}S$) which satisfies the equation

$$-\frac{\hbar^2}{2m^*}\left\{\sum_{i,j=1}^{2}\frac{1}{\sqrt{g}}\frac{\partial}{\partial q_i}\left[\sqrt{g}\,\overline{g}_{i,j}\,\frac{\partial}{\partial q_j}\sigma(q_1, q_2)\right] + \left(\frac{T^2}{4} - D\right)\sigma(q_1, q_2)\right\} = (E^S - E_n^N)\sigma(q_1, q_2) \tag{21}$$

where

$$\mathbf{g} = (g_{i,j}) = (\partial\vec{r}/\partial q_i \cdot \partial\vec{r}/\partial q_j)$$

is the metric tensor on the surface, $g = \det\mathbf{g}$, $\overline{g}_{i,j}$ the ratio between the algebraic complement of the element $g_{i,j}$ and g, T the double of the surface average curvature with changed sign, D the surface Gauss curvature [32], E^S the surface-state energy and E_n^N the energy of the motion along the surface normal. Equation (21) shows that a topological potential appears, which depends on the mean and Gauss surface curvature. This potential is, as we will show in the next section, responsible for the particle confinement at the surface points of largest curvature. It must be pointed out that if we had considered a particle moving on the surface (that is, in a two-dimensional world) the Schrödinger equation would not have contained this contribution [22].

In our case the curvilinear coordinate system on the surface is $(q_1, q_2) = (\Theta, \Phi)$ where Θ and Φ are defined in equation (1). This system is orthogonal (that is, $g_{1,2} = g_{2,1} = 0$) and because of the surface invariance with respect to the q_2-coordinate, $g_{1,1}$ and $g_{2,2}$ do not depend on q_2. Therefore equation (21) becomes

$$-\frac{1}{g_{1,1}}\frac{\partial^2}{\partial q_1^2}\sigma(q_1, q_2) - \frac{1}{\sqrt{g_{1,1}g_{2,2}}}\frac{\partial}{\partial q_1}\left[\sqrt{\frac{g_{2,2}}{g_{1,1}}}\right]\frac{\partial}{\partial q_1}\sigma(q_1, q_2) - \frac{1}{g_{2,2}}\frac{\partial^2}{\partial q_2^2}\sigma(q_1, q_2) - \left(\frac{T^2}{4} - D\right)\sigma(q_1, q_2) = \frac{2m^*}{\hbar^2}(E^S - E_n^N)\sigma(q_1, q_2). \tag{22}$$

Equation (22) contains terms in the second derivatives with respect to q_1 and q_2 and a term in the first derivative with respect to q_1. This latter can be eliminated with the substitution

$$\sigma(q_1, q_2) = \left(\frac{g_{1,1}}{g_{2,2}}\right)^{1/4} t(q_1)\exp(\mathrm{i}mq_2) \tag{23}$$

where we have taken in account also the fact that, because of the surface symmetry, equation (22) is separable and its solution must be an eigenfunction of the z-component of the angular momentum with eigenvalues $m\hbar$ ($m = 0, \pm1, \pm2, \ldots$). Using the surface parametric equations (1) we get $g_{1,1} = a^2\cos^2\Theta + c^2\sin^2\Theta$ and $g_{2,2} = a^2\sin^2\Theta$, so the motion of the particle along the surface satisfies the Schrödinger-like equation

$$-\frac{\mathrm{d}^2t}{\mathrm{d}\Theta^2} - \left[\frac{1 + (6\chi^2 - 2)\tan^2\Theta + (8\chi^2 - 3)\tan^4\Theta + \chi^2(3 + \chi^4 - 2\chi^2)\tan^6\Theta}{4(1 + \chi^2\tan^2\Theta)^2\tan^2\Theta} - m^2\left(\chi^2 + \frac{1}{\tan^2\Theta}\right)\right]t(\Theta) = \frac{\varepsilon^S c^2}{\chi^2}\frac{1 + \chi^2\tan^2\Theta}{1 + \tan^2\Theta}t(\Theta) \tag{24}$$

with a position-dependent effective mass given by

$$m^S(\Theta) = m^*(1 + \chi^2 \tan^2\Theta)/\chi^2(1 + \tan^2\Theta).$$

We have set $\varepsilon^S = 2m^*(E^S - E_n^S)/\hbar^2$. Because as $\chi \to 1$ the solutions of equation (24) become the associated Legendre functions, it is possible to label the eigenvalues and eigenfunctions with two indexes l and m with $m = 0, \pm1, \pm2, \ldots$ and $l = |m|, |m|+1, |m|+2, \ldots$ ($\varepsilon^S \equiv \varepsilon^S_{l,m}$, $t(\Theta) \equiv t_{l,m}(\Theta)$ and $\sigma(\Theta, \Phi) \equiv \sigma_{l,m}(\Theta, \Phi)$).

5. Numerical results and discussion

Using the separation constant expansions for $h \to 0$ and $h \to +\infty$ given in the appendix, we have solved equations (8*a*) and equation (14*a*) numerically using a mid-point shooting method with the boundary condition $J(\bar{\xi}) = 0$. With the same method we have solved equation (20). In figure 1(a) we show the comparison between the ground-state energy (as a function of χ) calculated with the exact method (full line) and the one calculated using the variational approach (dashed line) given in section 3. As we can see, the results are in very good accord

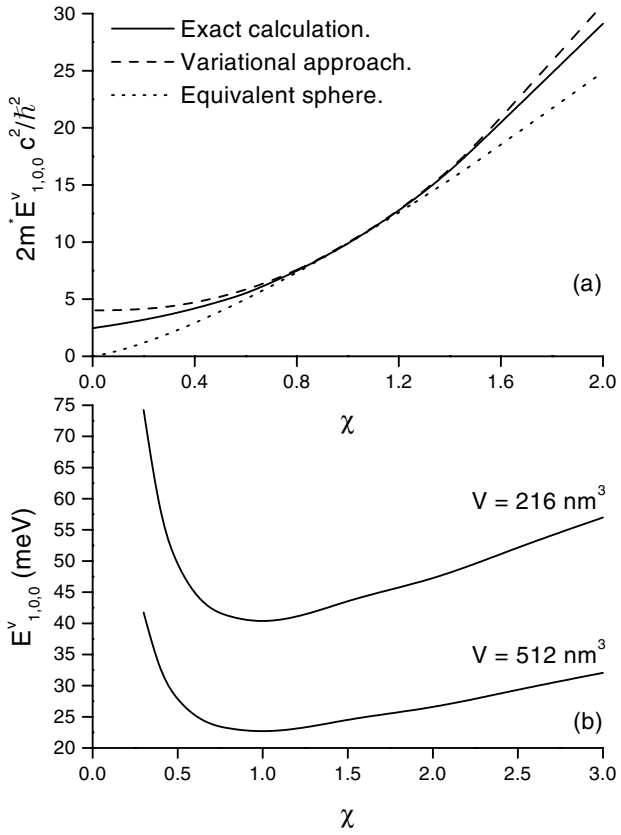

Figure 1. (a) The ground-state energy for a particle confined in an ellipsoidal quantum dot as calculated with the exact approach (full line) and the variational one (dashed line). The volume-confinement energy of the equivalent sphere is also shown for comparison (dotted line). (b) The volume-confined ground-state energy is shown for two families of ellipsoids with constant volumes $V = 216\,\text{nm}^3$ and $V = 512\,\text{nm}^3$ as a function of the degree of anisotropy χ. The shape dependence of this energy clearly comes out.

provided that we do not consider geometries with χ very far from 1. Anyway, as expected, the variational solution always gives an upper bound for the exact one. Moreover, we can see that these energies are an increasing function of χ, as they should be. In fact, the confinement energy of a particle in a volume V behaves as $V^{-2/3}$ and, since the ellipsoid-to-sphere volume ratio is $1/\chi^2$ (we mean the sphere of radius c which in figure 1(a) is represented by the point $\chi = 1$), we expect the ellipsoid ground-state energy to be smaller than the corresponding energy for the sphere if $\chi < 1$ and vice versa if $\chi > 1$. The result confirms this statement, but it must be pointed out that we cannot attribute it to a pure volume effect (that is, the smaller the volume, the bigger the energy). In order to clarify this point, in the same figure we have also shown (dotted line) the energy that we get if we consider the equivalent sphere—that is, the sphere with a volume equal to the ellipsoid volume. If we indicate as R_{eq} the radius of this sphere we have

$$\frac{4}{3}\pi R_{eq}^3 = \frac{4}{3}\pi a^2 c \Rightarrow R_{eq} = \frac{c}{\chi^{2/3}}. \tag{25}$$

The results shown in figure 1(a) demonstrate that, apart from in a very small region around $\chi = 1$, the equivalent-sphere energy is always below that of the ellipsoid. This means that the deformation and the anisotropy effects (that is, the geometry deviations with respect to the sphere) play a very important role in determining the energy spectrum of our system and that the correct interpretation of the confined-system properties as experimentally determined should take into account not only its mean dimensions but also its geometry. In order to give a quantitative estimation of how the shape can modify the system properties, in figure 1(b) the volume-confined ground-state energy is shown as a function of the degree of anisotropy χ for two different ellipsoid families with constant volume ($V = 216$ nm^3 and $V = 512$ nm^3). If $\chi = 1$ we get the energies for spheres with radii $a = c = 6$ nm and $a = c = 8$ nm respectively. We have used the spherical conduction band effective mass for silicon, which is $m^* = 0.2588 m_e$ if m_e is the free-electron mass. Two effects clearly emerge. The first one is a volume effect, which corresponds to the fact that for fixed χ the bigger the volume the lower the confinement energy. The second and the most important one is a shape effect—that is, the strong dependence of this energy on the structure geometry. In particular, for a fixed volume the spherical geometry ($\chi = 1$) shows the lowest value of the energy while it is larger for anisotropic structures ($\chi \neq 1$).

In figure 2 we show the energy as a function of χ for the ground state ($n = l = m = 0$, full line) and the first two excited states ($n = m = 0$, $l = 1$, dotted line and $n = 0$, $l = |m| = 1$, dashed line). All of these states correspond to $n = 0$ which means that there are no nodes in the radial part of the wave function. The degeneracy of the states with $l = 1$ and $|m| = 0, 1$ for $\chi = 1$ is removed by the deformation effects. The only degeneracy that we have is again with respect to $|m|$. It is very interesting to note that all the states shown become degenerate as $\chi \to 0$. The explanation of this behaviour is that, because we are considering the quantity $2m^* E^v c^2/\hbar^2$—that is, the energy with fixed c—the limit shown corresponds to $a \to +\infty$. In this limit we get two parallel planes with separation $2c$ for which the ground-state energy is $(\hbar^2/2m^*)(\pi/2c)^2$ in complete accord with the result obtained. Higher excited states with fixed n (that is, with a fixed number n of nodes in the radial part of the wave function) are all degenerate in this limit, simply because for the parallel-plane system the confinement energy depends only on the number of nodes of the wave function in the direction normal to them. A similar argument can be used to explain why, as we have checked, the states with the same n and $|m|$ but different l are all degenerate with the value of $2m^* E^v a^2/\hbar^2 = (2m^* E^v c^2/\hbar^2)/\chi^2$ given by $Z_{m,n}^2$ where $Z_{m,n}$ is the nth zero of the mth Bessel cylindrical function as $\chi \to +\infty$. In fact, in this limit and for fixed a (that is, $c \to +\infty$) we get a cylinder of radius a for which the confinement energies depend just on $Z_{m,n}^2$ (or, in other words, on the z-component of the

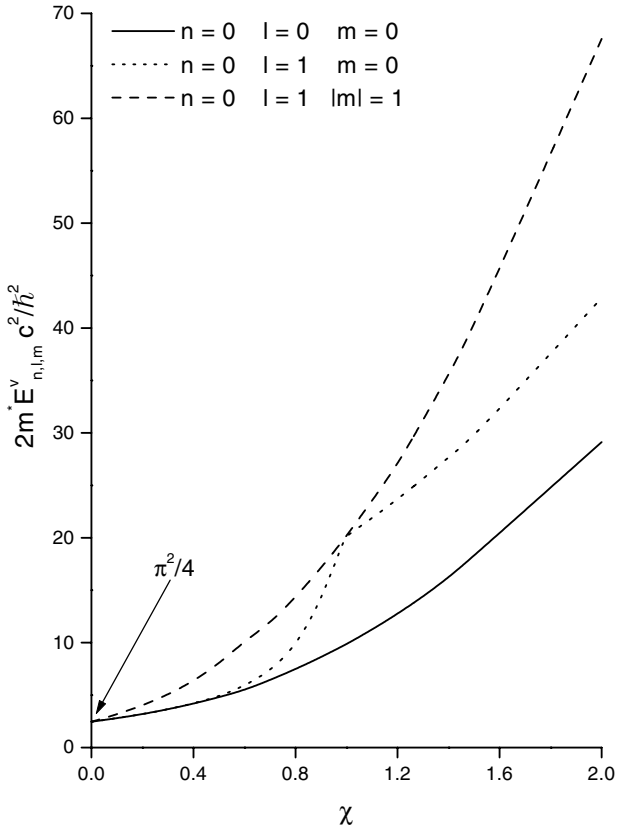

Figure 2. The particle energy as a function of χ is shown for the ground state ($n = l = m = 0$, full line) and the first two excited states $l = 1$, $n = m = 0$ (dotted line) and $n = 0$, $l = |m| = 1$ (dashed line). The arrow indicates that for fixed c and $\chi \to 0$ the energy of all of these states is $\pi^2/4$—that is, that of the volume-confined ground state of two parallel planes with separation $2c$.

angular momentum and the number of nodes of the radial wave function inside the cylinder). These two limiting results confirm the validity of our procedure.

In figure 3 we show the dependence on Θ ($\eta = \cos\Theta$) of the ground-state wave function calculated numerically by solving the angular equations (14*b*) and (8*b*) with $\chi = 0.5$ (a) and $\chi = 1.5$ (b) respectively. In the first case (and, more generally, for $\chi < 1$) we find the state more confined around the positions $\Theta = 0$ and $\Theta = \pi$ (panel (a)) while in the second one (and, more generally, for $\chi > 1$) it is at $\Theta = \pi/2$ (panel (b)). This is an example of how the wave-function localization depends on the dot geometry.

As has been explained in section 4, we have also investigated topological surface states. In figure 4(a) we show the energy spectrum calculated by solving numerically equation (24). The ground state with $l = m = 0$ (full line) and the first two excited states ($m = 0$, $l = 1$, dotted line and $l = |m| = 1$, dashed line) are shown. These latter two are degenerate for $\chi = 1$, in which case the ellipsoid is degenerate with a sphere and the wave functions become the spherical harmonics $Y_l^m(\Theta, \Phi)$ with energies $\hbar^2 l(l+1)/2m^* R^2$ (if R is the sphere radius). In particular for $\chi = 1$ the ground state has zero energy which corresponds to the fact that the topological potential, being vanishing, is unable to localize the wave function along the surface. We have also performed the calculation of the ground-state energy using the variational

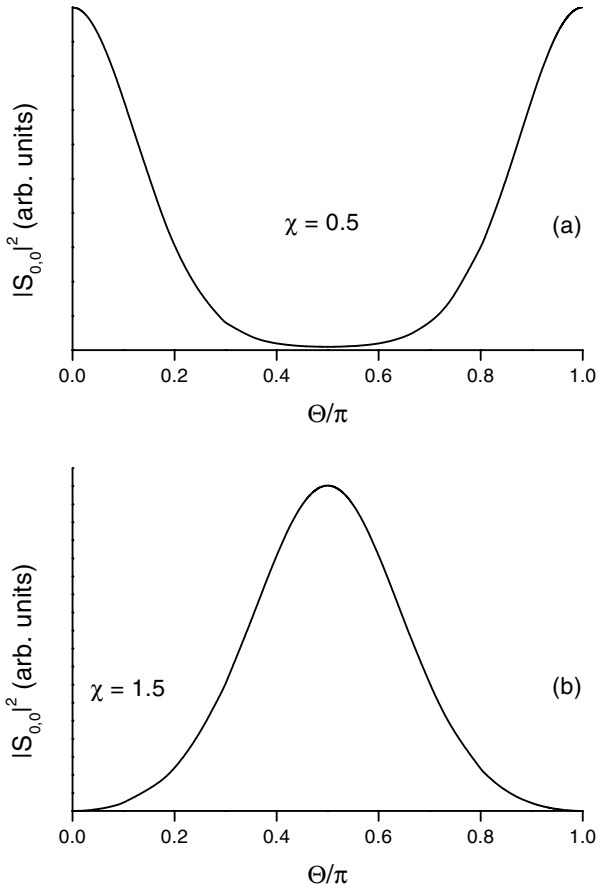

Figure 3. The dependence on Θ of the volume-confined ground-state wave function as calculated with the variational procedure is shown for $\chi = 0.5$ (a) and $\chi = 1.5$ (b). The particle localizes at the positions $\Theta = 0$ and $\Theta = \pi$ or $\Theta = \pi/2$ depending on whether $\chi < 1$ or $\chi > 1$ respectively.

method. An inspection of the effective potential of equation (24) suggests that a good choice of trial function can be

$$\widetilde{t}_0(\Theta) = \sqrt{(\sin\Theta)}\exp(\alpha\cos^2\Theta) \tag{26}$$

were α is a variational parameter which must be determined from the condition of minimum energy. In figure 4(b) we show the ground-state energy (full line) and the value of the variational parameter (dashed line) as functions of χ which have been determined in this way. This ground-state energy always represents, as it has to, an upper bound to the exact one (shown in figure 4(a)) and is in very good accord with it.

It is of interest to compare the energies of volume-confined states with those which are surface localized. Before such a comparison, it must be stressed that the surface energies that we have calculated are not 2D energies, as one could erroneously believe, simply because they have been derived starting from a 3D Hamiltonian. Comparing the ground-state energy for the volume-confined states (see figure 2) and surface states (see figure 4(a)) we can see that these latter are always (that is, for any χ) below the first ones, confirming what we found for a completely different geometry (a deformed quantum wire) with an unlimited surface [22]. In figure 5 we show the surface ground-state wave function calculated for $\chi = 4.0$ (a), $\chi = 2.5$ (b)

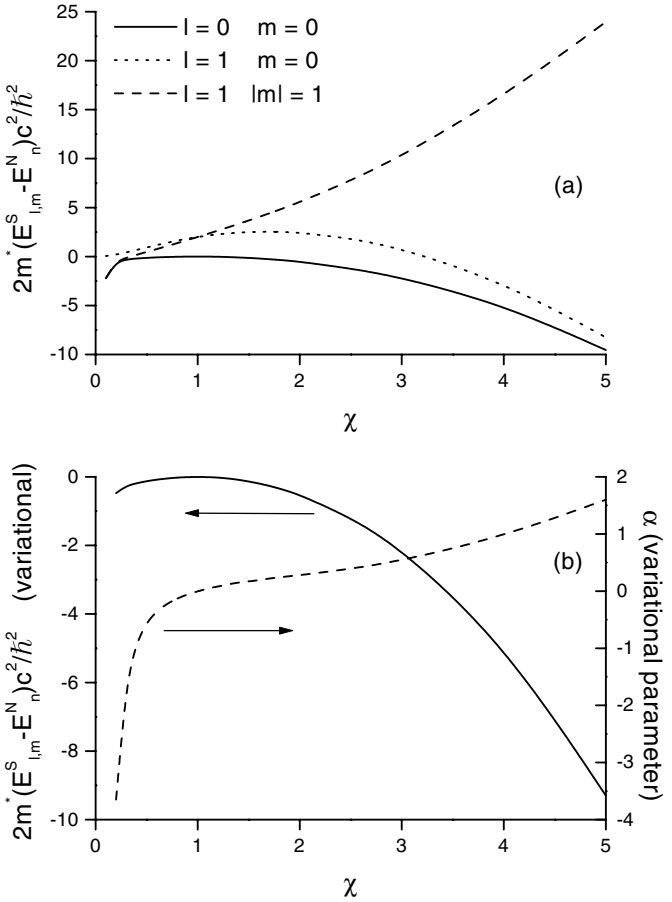

Figure 4. (a) The topological surface-state energy is shown for the ground state $l = m = 0$ (full line) and the first two excited states $l = 1$, $m = 0$ (dotted line) and $l = |m| = 1$ (dashed line). (b) The ground-state energy as calculated using the variational method (full line) and the corresponding variational parameter (dashed line) are shown.

and $\chi = 0.5$ (c). It can be seen that for values of $\chi > 1$ the surface state tends to localize at the positions $\Theta = 0$ and $\Theta = \pi$, while if $\chi < 1$ we find a state localized at $\Theta = \pi/2$. This means that the 'Θ-localization' of the surface state is opposite to that of the volume-confined state.

6. Conclusions

The anisotropy effects in ellipsoidal quantum dots have been shown for both volume-confined and topological surface states. The results presented clearly show that the volume-confined energy level structure is modified with respect to that of the spherical quantum dot, giving rise, in particular, to a splitting of the $l = 1$ states. Therefore, experimental evidence for anisotropy should come out on observing optical transitions between excited states and the polarization of the emitted light [33]. Moreover, we have shown that even for the ground-state energy it is not possible to give a description in terms of an 'equivalent' spherical dot, giving evidence for the strong correlation between volume effects and the system geometry. In fact, volume-confined

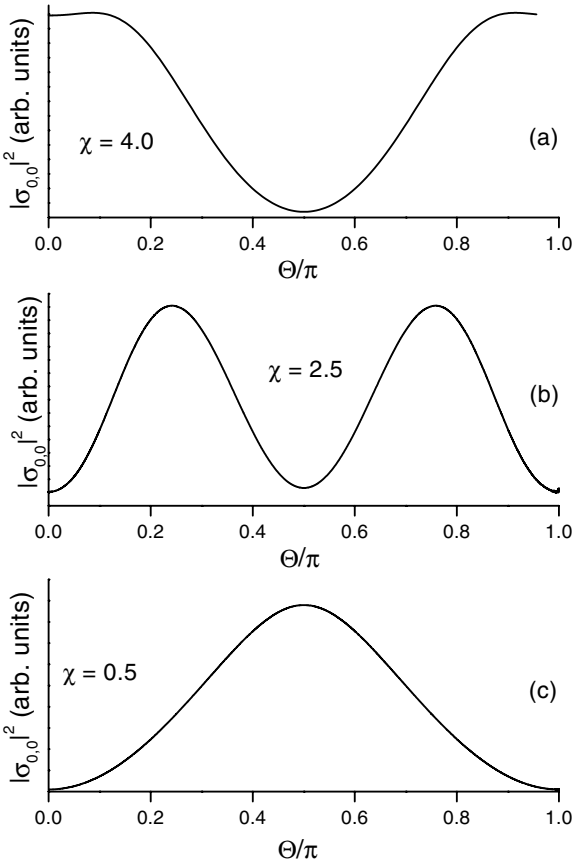

Figure 5. Surface-ground-state wave functions for $\chi = 4.0$ (a), $\chi = 2.5$ (b) and $\chi = 0.5$ (c). The particle localization as a function of χ behaves in the opposite way to that for a volume-confined ground state.

energies relative to structures with constant volume have been compared; it emerges that they have greater values when the degree of anisotropy is higher. This means that for a fixed volume the spherical quantum dot shows the lowest band-gap shift. The validity of our calculations has been checked also for the limiting cases $\chi \to +\infty$ (with fixed a) and $\chi \to 0$ (with fixed c), in which all the degeneracies are modified in order to obtain, respectively, the cylindrical quantum wire and the slab-confined energy levels.

Finally, topological surface states, completely absent for the spherical geometry, appear, confirming their topological nature—that is, their strong dependence on the surface curvature variations. In particular, the ground state has been shown to lie always below the volume-confined one, and the respective 'Θ-localizations' to be different. This means that the possibility of charge transfer from the bulk to this particular class of surface states should be less efficient than that in deformed quantum wires [22].

Acknowledgment

G Cantele was supported by the European Social Found.

Appendix A. Separation constant expansions

Inserting the wave-function series expansions (9) and (10) in the respective equations (8*a*) and (8*b*) it is possible to derive the recurrence formulae for the expansion coefficients $a_s^{l,m}$ and $d_s^{l,m}$. In particular it is possible to show that they are not independent, because they satisfy the relation [26]

$$a_s^{l,m}(h) = (-1)^{(l-|m|-s)/2}\frac{(s+2|m|)!}{s!}\frac{(l-|m|)!}{(l+|m|)!}d_s^{l,m}(h). \tag{A.1}$$

In order to unequivocally determine these coefficients we must obviously give a normalization condition. In particular the radial part of the wave function can be normalized in such a way that $je_{l,m}(h,\xi) \to j_l(h\xi)$ as $\xi \to +\infty$ (in which case $f\sqrt{\xi^2-1} \simeq f\xi$ and the ellipsoids tend to a sphere) [26]. For the angular part the normalization can be done by requiring that $S_{l,m}(h,\eta) \to P_l^{|m|}(\eta)$ as $\eta \to 1$; that is, the value of the spheroidal angular wave function for $\eta = 1$ can be taken as the same as the value of the corresponding associated Legendre function at the same point. This gives the further conditions

$$\sum_{s=0,1}^{+\infty\,\prime}(-1)^{(l-|m|-s)/2}a_s^{l,m}(h) = 1 \tag{A.2}$$

and

$$\sum_{s=0,1}^{+\infty\,\prime}\frac{(s+2|m|)!}{s!}d_s^{l,m}(h) = \frac{(l+|m|)!}{(l-|m|)!}. \tag{A.3}$$

It is possible to find the numerical values for the first coefficients of the expansions (9) and (10) in reference [26].

Moreover, by requiring the angular solution $S_{l,m}(h,\eta)$ to be regular at $\eta = \pm 1$ it is possible to derive for fixed h, l and m the corresponding A-value (in fact, it turns out that for most values of A the solution is finite at $\eta = 1$ but infinite at $\eta = -1$; the recursion equation can be solved using the continued-fraction technique [34] which gives the discrete set of the A-values such that the series converges). In this way we can get an expansion of the separation constant as $h \to 0$ and $h \to \infty$. If $\chi > 1$ the separation constant can be written as follows:

$$A_{l,m}(h) = \sum_{k=0}^{4}\alpha_{2k}^{l,m}h^{2k} + \mathrm{O}(h^{10}) \tag{A.4}$$

where

$$\begin{aligned}
\alpha_0^{l,m} &= l(l+1)\\
\alpha_2^{l,m} &= \frac{1}{2}\left[1 - \frac{(2|m|-1)(2|m|+1)}{(2l-1)(2l+3)}\right]\\
\alpha_4^{l,m} &= \frac{-(l-|m|+1)(l-|m|+2)(l+|m|+1)(l+|m|+2)}{2(2l+1)(2l+3)^3(2l+5)}\\
&\quad + \frac{(l-|m|-1)(l-|m|)(l+|m|-1)(l+|m|)}{2(2l-3)(2l-1)^3(2l+1)}\\
\alpha_6^{l,m} &= (4m^2-1)\left[\frac{(l-|m|+1)(l-|m|+2)(l+|m|+1)(l+|m|+2)}{(2l-1)(2l+1)(2l+3)^5(2l+5)(2l+7)}\right.\\
&\quad \left. - \frac{(l-|m|-1)(l-|m|)(l+|m|-1)(l+|m|)}{(2l-5)(2l-3)(2l-1)^5(2l+1)(2l+3)}\right]\\
\alpha_8^{l,m} &= 2(4m^2-1)^2\Gamma_0^{l,m} + \frac{\Gamma_1^{l,m}}{16} + \frac{\Gamma_2^{l,m}}{8} + \frac{\Gamma_3^{l,m}}{2}
\end{aligned} \tag{A.5a}$$

$$\Gamma_0^{l,m} = \frac{(l-|m|-1)(l-|m|)(l+|m|-1)(l+|m|)}{(2l-5)^2(2l-3)(2l-1)^7(2l+1)(2l+3)^2} - \frac{(l-|m|+1)(l-|m|+2)(l+|m|+1)(l+|m|+2)}{(2l-1)^2(2l+1)(2l+3)^7(2l+5)(2l+7)^2}$$

$$\Gamma_1^{l,m} = \frac{(l-|m|-3)(l-|m|-2)(l-|m|-1)(l-|m|)}{(2l-7)(2l-5)^2(2l-3)^3(2l-1)^4(2l+1)} \times (l+|m|-3)(l+|m|-2)(l+|m|-1)(l+|m|) - \frac{(l-|m|+1)(l-|m|+2)(l-|m|+3)(l-|m|+4)}{(2l+1)(2l+3)^4(2l+5)^3(2l+7)^2(2l+9)} \times (l+|m|+1)(l+|m|+2)(l+|m|+3)(l+|m|+4) \tag{A.5b}$$

$$\Gamma_2^{l,m} = \frac{(l-|m|+1)^2(l-|m|+2)^2(l+|m|+1)^2(l+|m|+2)^2}{(2l+1)^2(2l+3)^7(2l+5)^2} - \frac{(l-|m|-1)^2(l-|m|)^2(l+|m|-1)^2(l+|m|)^2}{(2l-3)^2(2l-1)^7(2l+1)^2}$$

$$\Gamma_3^{l,m} = \frac{(l-|m|-1)(l-|m|)(l-|m|+1)(l-|m|+2)}{(2l-3)(2l-1)^4(2l+1)^2(2l+3)^4(2l+5)} \times (l+|m|-1)(l+|m|)(l+|m|+1)(l+|m|+2)$$

as $h \to 0$, while

$$A_{l,m}(h) = \beta_0^{l,m} - \sum_{k=1}^{5} \frac{\beta_k^{l,m}}{h^k} + \mathrm{O}(h^{-6}) \tag{A.6}$$

where

$$\begin{aligned}
\beta_0^{l,m} &= q_{l,m}h + m^2 - \frac{1}{8}(q_{l,m}^2+5) \\
\beta_1^{l,m} &= \frac{q_{l,m}}{64}(q_{l,m}^2 + 11 - 32m^2) \\
\beta_2^{l,m} &= \frac{1}{1024}\left[5(q_{l,m}^4 + 26q_{l,m}^2 + 21) - 384m^2(q_{l,m}^2+1)\right] \\
\beta_3^{l,m} &= \frac{1}{128^2}(33q_{l,m}^5 + 1594q_{l,m}^3 + 5621q_{l,m}) - \frac{m^2}{128}(37q_{l,m}^3 + 167q_{l,m}) + \frac{m^4}{8}q_{l,m} \\
\beta_4^{l,m} &= \frac{1}{256^2}(63q_{l,m}^6 + 4940q_{l,m}^4 + 43327q_{l,m}^2 + 22470) \\
&\quad - \frac{m^2}{512}(115q_{l,m}^4 + 1310q_{l,m}^2 + 735) + \frac{3m^4}{8}(q_{l,m}^2+1) \\
\beta_5^{l,m} &= \frac{1}{1024^2}(527q_{l,m}^7 + 61529q_{l,m}^5 + 1043961q_{l,m}^3 + 2241599q_{l,m}) \\
&\quad - \frac{m^2}{32768}(5739q_{l,m}^5 + 127550q_{l,m}^3 + 298951q_{l,m}) \\
&\quad + \frac{m^4}{512}(355q_{l,m}^3 + 1505q_{l,m}) - \frac{m^6 q_{l,m}}{16} \\
q_{l,m} &= 2(l-|m|)+1
\end{aligned} \tag{A.7}$$

as $h \to \infty$.

If $\chi < 1$ the expansion as $h \to 0$ becomes

$$A_{l,m}(h) = \sum_{k=0}^{4}(-1)^k \alpha_{2k}^{l,m} h^{2k} + \mathrm{O}(h^{10}) \tag{A.8}$$

with the coefficients $\alpha_{2k}^{l,m}$ given by equation (A.5*a*), while the expansion as $h \to \infty$ becomes

$$A_{l,m}(h) = \gamma_0^{l,m} - \sum_{k=1}^{4} \frac{\gamma_k^{l,m}}{h^k} + \mathrm{O}(h^{-5}) \tag{A.9}$$

where

$$\begin{aligned}
\gamma_0^{l,m} &= -h^2 + 2h(2\nu + |m| + 1) - 2\nu(\nu + |m| + 1) - (|m| + 1) \\
\gamma_1^{l,m} &= \frac{Q_{l,m}(Q_{l,m}^2 + 1 - m^2)}{2^3} \\
\gamma_2^{l,m} &= \frac{5Q_{l,m}^4 + 10Q_{l,m}^2 + 1 - 2m^2(3Q_{l,m}^2 + 1) + m^4}{2^6} \\
\gamma_3^{l,m} &= \frac{Q_{l,m}\left[33Q_{l,m}^4 + 114Q_{l,m}^2 + 37 - 2m^2(23Q_{l,m}^2 + 25) + 13m^4\right]}{2^9} \\
\gamma_4^{l,m} &= \frac{1}{2^{10}}(63Q_{l,m}^6 + 340Q_{l,m}^4 + 239Q_{l,m}^2 + 14 - 10m^2(10Q_{l,m}^4 + 23Q_{l,m}^2 + 3) \\
&\quad + m^4(39Q_{l,m}^2 - 18) - 2m^6)
\end{aligned} \tag{A.10a}$$

and

$$\nu = \begin{cases} \dfrac{l - |m|}{2} & \text{for } l - |m| \text{ even} \\ \dfrac{l - |m| - 1}{2} & \text{for } l - |m| \text{ odd} \end{cases} \tag{A.10b}$$

$$Q_{l,m} = \begin{cases} l + 1 & \text{for } l - |m| \text{ even} \\ l & \text{for } l - |m| \text{ odd.} \end{cases}$$

These expansions are given in reference [28]. It must be pointed out that the numerical solution of equations (8*a*) and (14*a*) requires the function $A_{l,m}(h)$. For this purpose we have used the expansions shown above, verifying that, if we stop them at the maximum order shown, there always exists an interval of values of h (depending, in general, on l and m) where the expansion as $h \to 0$ and the one as $h \to \infty$ give in practice the same values for the separation constant. In particular we have found, for fixed l and m, the matching point of the two expansions. This means that without any appreciable error we can have the values of the separation constant for h varying throughout the range $(0, +\infty)$.

References

[1] Wegscheider W, Schedelbeck G, Bichler M and Abstreiter G 1998 *Physica* E **3** 103 and references therein
[2] Zhuang Lei, Guo Lingjie and Chou S Y 1998 *Appl. Phys. Lett.* **72** 1205
[3] Grundmann M 2000 *Physica* E **5** 167
[4] Proot J P, Delerue C and Allan G 1992 *Appl. Phys. Lett.* **61** 1948
[5] Hill N A and Whaley K B 1995 *Phys. Rev. Lett.* **75** 1130
[6] Delerue C, Lannoo M and Allan G 1996 *Phys. Rev. Lett.* **76** 3038
[7] Wang Lin-Wang and Zunger A 1994 *J. Phys. Chem.* **98** 2158
[8] Ögüt S, Chelikowsky J R and Louie S G 1997 *Phys. Rev. Lett.* **79** 1770
[9] Bastard G 1981 *Phys. Rev.* B **24** 5693
[10] Yoffe A D 1993 *Adv. Phys.* **42** 173 and references therein
[11] Rama Krishna M V and Friesner R A 1991 *Phys. Rev. Lett.* **67** 629
[12] Mizel A and Cohen M L 1997 *Phys. Rev.* B **56** 6737
[13] Mizel A and Cohen M L 1998 *Phys. Rev.* B **57** 9515
[14] Braginsky L S 1999 *Phys. Rev.* B **60** R13 970
[15] Ninno D, Iadonisi G, Buonocore F and Cantele G 2000 *Sensors Actuators* B at press

[16] Brus L E 1984 *J. Chem. Phys.* **80** 4403
[17] Peng Xiaogang, Manna L, Yang W, Wickham J, Scher E, Kadavanich A and Alivisatos A P 2000 *Nature* **404** 59
[18] Cusack M A, Briddon P R and Jaros M 1996 *Phys. Rev.* B **54** R2300
[19] Petterson H, Warburton R J, Kotthaus J P, Carlsson N, Seifert W, Pistol M-E and Samuelson L 1999 *Phys. Rev.* B **60** R11 289
[20] Ezaki T, Mori N and Hamaguchi C 1997 *Phys. Rev.* B **56** 6428
[21] Efros Al L and Rodina A V 1993 *Phys. Rev.* B **47** 10 005
[22] Cantele G, Ninno D and Iadonisi G 2000 *Phys. Rev.* B **61** 13 730
[23] da Costa R C T 1981 *Phys. Rev.* A **23** 1982
[24] Encinosa M and Etemadi B 1998 *Phys. Rev.* A **58** 77
[25] Ninno D, Iadonisi G and Buonocore F 1999 *Solid State Commun.* **112** 521
[26] Stratton J A, Morse P M, Chu L J, Little J D C and Corbatò F J 1956 *Spheroidal Wave Functions* (New York: Wiley)
[27] Bianchi L 1904 *Lezioni di Geometria Differenziale* (Bologna: Nicola Zanichelli Editore) p 85
[28] Abramowitz M and Stegun I A 1972 *Handbook of Mathematical Functions* (New York: Dover)
[29] Kupriyanov L Yu (ed) 1996 *Semiconductor Sensors in Physico-Chemical Studies* (Amsterdam: Elsevier Science)
[30] Ando T, Fowler A B and Stern F 1982 *Rev. Mod. Phys.* **54** 437
[31] Fujii H, Kanemaru S, Matsukawa T and Itoh J 1999 *Appl. Phys. Lett.* **75** 3986
[32] For the quantities related to the surface topology see, for instance
Smirnov V I 1964 *A Course of Higher Mathematics* vol II (New York: Pergamon)
[33] Kovalev D, Ben-Chorin M, Diener J, Averboukh B, Polisski G and Koch F 1997 *Phys. Rev. Lett.* **79** 119
[34] Morse P M and Feshbach H 1953 *Methods of Theoretical Physics* (New York: McGraw-Hill)